Combustion and Flame 187 (2018) 96–104

Contents lists available at ScienceDirect

Combustion and Flame

journal homepage: www.elsevier.com/locate/combustflame

Highly stable functionalized aluminum nanoparticles for magneto-energetic composite fabrication

Van Tan Tran[a], Ji Hoon Kim[b], Ki-Jae Jeong[a], Junyoung Kwon[a], Soo Hyung Kim[b,*], Jaebeom Lee[a,*]

[a] Department of Cogno-Mechatronics Engineering, Pusan National University, Busan 609-735, Republic of Korea
[b] Department of Nano Fusion Technology, Pusan National University, Busan 609-735, Republic of Korea

ARTICLE INFO

Article history:
Received 1 March 2017
Revised 23 March 2017
Accepted 12 September 2017

Keywords:
Aluminum
Surface functionalization
Magneto-energetic
Composite

ABSTRACT

An effective coating strategy is employed to functionalize and protect the surfaces of aluminum (Al) nanoparticle (NPs) from oxidation and aggregation using silanization of the oxide surface with (3-aminopropyl) triethoxysilane (Al@APTES), followed by an amine/carboxylic exchange using glutaric anhydride (Al@APTES@GA). The stability of the two types of functionalized Al NPs in aqueous solution is studied using dynamic light scattering and x-ray diffraction phase/composition identification. It is found that Al@APTES NPs transform into bayerite (β-$Al(OH)_3$) after storage for a short period of time, while Al@APTES@GA NPs exhibit long-term stability. Hydration of Al results in micro-sized aggregates and a large proportion of dead weight, which reduces the particles' energetic properties. Al–Fe_3O_4 magnetic–energetic (Magnerg) composites are fabricated via the electrostatic interaction of oppositely charged NPs in an aqueous solution. The high dispersity and stability of Al@APTES@GA NPs assure their intimate arrangement with oxidizing Fe_3O_4 NPs that facilitates mass transport between reactants.

1. Introduction

Aluminum is known to be one of the best energetic metals, and has attracted intense interest as a research topic for military applications [1,2], as well as for civilian purposes [3]. Though the use of nanoscale Al can enhance the overall reactivity of the material, Al nanoparticles are susceptible to aggregation and spontaneous oxidation, which inhibit the formation of homogeneous and energetic nanocomposites. Additionally, as the Al particle size is reduced, the passivated-oxide layer that forms begins to represent a significant portion of the particle mass. Oxidation of the particle continues further to the inner core even after the outer passivated oxide layer is completely formed. Various coating methods have been used to overcome these issues using carboxylic acids [4], organosilanes [5,6], diazonium chemistry [7], or phosphonic acids [8], organosilane compounds such as trichloro-, trimethoxy- or triethoxysilanes have been used most extensively due to their great affinity for the metal-oxide shell. Nevertheless, these coatings are either unstable (in the case of short alkyl chains of amino-terminated silanes) or unfavorable in aqueous solutions (in the case of long alkyl chains of amino-terminated or alkyl-terminated silanes) due to solubility [9].

Generally, oxidizers such as MoO_3 [10], CuO [11], Fe_2O_3 [12], and Co_3O_4 [13] are used in combination with fuel, i.e., Al, in order to significantly enhance reactivity. The most convenient way of creating a composite is by physically mixing solid fuel and oxidizer. However, the mass transfer process in these composites may act as a rate limiting step due to poor dispersion of the oxidizer and fuel NPs, which inhibits the rate of energy release [14]. More sophisticated assembly methods including sol–gel [15], electrospraying [11], electrostatic-directed assembly [16] and sputtering [17] have been employed to produce controllable assembled composites [11,18–21]. Polymers have also been employed as linkers to assemble fuel into an oxidizer matrix [22]. More recently, a DNA-directed assembly approach has been demonstrated, in which two types of NPs were coated with single-stranded DNA molecules of complementary sequences to produce highly energetic nanocomposites [23]. These different methods have allowed the generation of micrometer-sized composites with intimate interfacial contacts between fuel and oxidizer, resulting in enhanced energetic performance.

Iron(III) oxide (Fe_2O_3) has been widely used to form a classical-thermite system with Al, which has led to the development of various applications such as welding, portable heat sources, pyrotechnics, and explosives [24]. In addition to Fe_2O_3, it was

* Corresponding authors.
E-mail addresses: sookim@pusan.ac.kr (S.H. Kim), jaebeom@pusan.ac.kr, nanoleelab@gmail.com (J. Lee).

https://doi.org/10.1016/j.combustflame.2017.09.014
0010-2180/

reported that the Al–Fe_3O_4 system also exhibits a highly exothermic reaction when subjected to thermal and/or mechanical treatments [25]. A great advantage of Fe_3O_4 over other oxidizers is its magnetic properties, which may facilitate assembly processes as well as introduce a method of controlling the direction of an explosion. Several researchers have studied the effects of magnetic fields on flames. In these cases, the magnetic effect has been explained by the movement of the reactants and reaction products in the presence of a magnetic-field gradient [26–28]. However, only minimal changes in combustion were caused by the application of magnetic fields to these flames [29]. Nanothermites for metal cutting and perforation require a highly directed or focused cutting flame derived from the activation of a thermite charge in order to effectively focus large amounts of energy on the desired cutting location. In general, thermite composites release heat in an isotropic regime that reduces the efficiency of the cutting/perforation process. One solution that has been proposed is the use of a nozzle with thermite cutting torches. This nozzle directs a maximized flow of cutting flame to the desired cutting location on a workpiece [30]. Controlled explosions are also important in building implosion since they can shorten the duration of work and reduce costs.

In this study, Al NPs are passivated and functionalized using silanization of the oxide surface with APTES (Al@APTES), followed by an amine/carboxylic exchange process using glutaric anhydride (GA) (Al@APTES@GA). The stability and dispersity of the two different kinds of Al particles in aqueous media are investigated. Citrate-coated and PEI-coated Fe_3O_4 NPs, which have negatively and positively charged surfaces, respectively, are employed to form electrostatically assembled structures with the functionalized Al NPs. We find enhanced energetic reactivity of the Al@APTES@GA composite compared with the Al@APTES one under different assembly durations.

2. Experimental section

2.1. Materials

Iron (III) chloride hexahydrate ($FeCl{\cdot}6H_2O$), trisodium citrate dihydrate ($C_6H_5Na_3O_7{\cdot}2H_2O$, Cit), sodium acetate ($CH_3COONa$, NaAc), branched polyethylenimine (PEI, average $M_W \sim 25{,}000$), glutaric anhydride (GA), (3-aminopropyl) triethoxysilane (APTES) and ethylene glycol (EG) were purchased from Sigma-Aldrich Inc. (Yong-In, South Korea). Aluminum nanoparticles with an average size of 80 nm were purchased from NT base Inc. (Yong-In, South Korea). Deionized (DI) water (> 18 MΩ cm^{-1}) was used for all solution preparations and experiments. All chemicals were analytical grade reagents and were used as received without further purification.

2.2. Synthesis of citrate-stabilized Fe_3O_4 (Fe_3O_4@Cit) NPs

$FeCl_3{\cdot}6H_2O$ (0.12 M) and trisodium-citrate dihydrate (34 mM) were first dissolved in ethylene glycol (20 mL). Next, anhydrous-sodium acetate (0.73 M) was added while the mixture was stirred. The mixture was stirred vigorously for 30 min and then sealed in a Teflon-lined stainless-steel autoclave (50 mL). The autoclave was heated at 200 °C and maintained at this temperature for 10 h, then allowed to cool to 25 °C. The black products were washed with ethanol and DI water several times, then dried at 60 °C for 6 h.

2.3. Synthesis of polyethylenimine-stabilized Fe_3O_4 (Fe_3O_4@PEI) NPs

$FeCl_3{\cdot}6H_2O$ (0.126 M) was first dissolved in EG (40 mL) to form a transparent solution. Anhydrous sodium acetate (NaAc) (3.6 g) was then added under continuous stirring until it was completely dissolved. The mixture was stirred vigorously for 30 min and then 1.2 g of PEI was added to the mixture. The mixture was heated to 60 °C for 20 min, then sealed in a Teflon-lined stainless-steel autoclave. The autoclave was heated at 220 °C and maintained at this temperature for 2 h. After this, it was allowed to cool to 25 °C. The black products were washed with ethanol and DI water several times and then dried at 60 °C for 6 h.

2.4. Stabilization of aluminum NPs

Amino-functionalized Al NPs (Al@APTES) were prepared through silanization of the aluminum surface with APTES. Al NPs (500 mg) were dispersed in absolute ethanol (50 mL) by sonicating for 10 min, followed by adding APTES (1.17 mL). The reaction was allowed to proceed under vigorous stirring for 4 h at 25°C. After that, the mixture was refluxed at 90°C for 1 h. The product was washed several times with ethanol, and then dried at 30°C in a vacuum oven. In order to functionalize the Al NPs with carboxylic groups, Al@APTES NPs (40 mg) were dissolved in ethanol (20 mL) and mixed with GA (0.2 M in ethanol, 20 mL). This mixture was stirred for 12 h at 25 °C to produce carboxyl-functionalized particles. The product was washed several times with ethanol then dried at 30 °C in a vacuum oven.

2.5. Fabrication of Magnerg composites

In a typical procedure, aqueous solutions of Al@APTES and Fe_3O_4@Cit NPs were prepared separately with a concentration of 10 mg mL^{-1}. The aqueous dispersion of Al@APTES NPs was admixed into that of Fe_3O_4@Cit NPs at 25°C at a volumetric ratio of 1:1. The mixture was vigorously shaken at 200 rpm for different-time durations: 30 min, 2 h, and 8 h. Finally, the product was washed with DI water with the help of a magnet, and then dried at 30 °C in a vacuum oven.

2.6. Explosion experiment

Open burn tests were performed to evaluate the energetic performance of Magnerg composites. Briefly, Magnerg composites (10 mg) in the form of loose powder were placed on the ignition stage. The Al–Fe_3O_4 composite powders were ignited by a heated tungsten wire coupled with an external-power supply. The entire process of burning the composites was recorded, using a high-speed camera (Photron, Model No. FASTCAM SA3 120 K) at a frame rate of 30 kHz.

2.7. Characterizations

The morphologies of the NPs and their assemblies were characterized via high-resolution transmission electron microscopy (HR-TEM) (JEOL, JEM-3010, Japan), and field-emission scanning electron microscopy (FE-SEM) (S-4700, Hitachi, Japan). Samples for TEM analysis were prepared by drop-casting a dilute solution of NPs onto ultrathin carbon-coated copper grids. The surface properties of the NPs were characterized via Fourier transform infrared (FT-IR) spectroscopy (JASCO, FTIR6300, Japan). TGA (TGA, SCINCO 1000, Korea) was performed in an N_2 gas environment (flow rate: 10 cm^3 min^{-1}) in a temperature range of 35–500 °C, at a heating rate of 10 °C min^{-1}. The surface potential and particle size distribution were measured using a zeta-sizer (ZS Nano, Malvern Instruments, UK). Magnetic measurements were performed using a superconducting quantum interference device (SQUID) magnetometer (MPMS XL-7, Quantum Design, Inc., San Diego, CA). X-ray diffraction (XRD) was performed on a PANalytical Empyrean X-ray Diffraction System with a Cu target ($\lambda = 1.540598$ Å) at a generator voltage of 40 kV, a generator current of 30 mA, and a scanning rate of 0.1° min^{-1}.

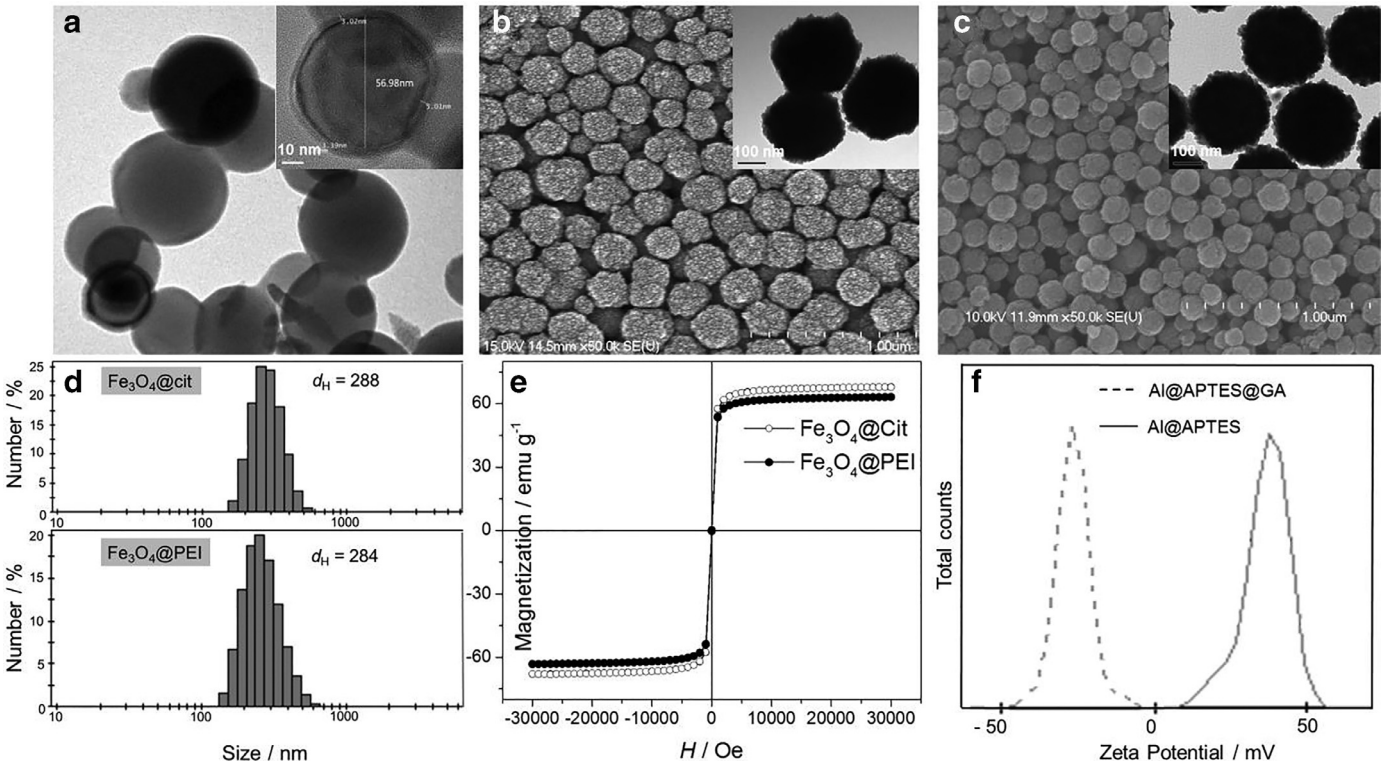

Fig. 1. SEM and TEM (inset) images of pristine Al (a), Fe_3O_4@Cit (b) and Fe_3O_4@PEI (c) particles and size distribution histgrams (d) and magnetic hysteresis curves at 300 K (e) of magnetic particles. Zeta potential of Al@APTES and Al@APTES@GA NPs (f).

3. Results and discussion

3.1. Surface modification and characterization of Al NPs

Pristine Al NPs with an average diameter of 80 nm with a thin alumina-shell are observed in Fig. 1(a). Fe_3O_4 NPs used as an oxidizer and stabilized with citrate and PEI are synthesized via a simple one-pot solvothermal method. Typical SEM and TEM images of Fe_3O_4@Cit and Fe_3O_4@ PEI particles isare shown in Fig. 1(b) and (c). Both kinds of Fe_3O_4 NPs appear to be similar in size with uniform-size distribution. Indeed, as shown in size distribution histogram in Fig. 1(d), Fe_3O_4@Cit and Fe_3O_4@PEI NPs are highly uniform with the hydrodynamic size of 288 nm and 284 nm, respectively. The magnetic properties of the Fe_3O_4 NPs were characterized using a superconducting quantum interference device (SQUID) and Fig. 1(e) shows typical hysteresis curves at 300 K of the magnetic NPs. Both of the NPs show superparamagnetism and saturation magnetization of 68 $emug^{-1}$ and 63 $emug^{-1}$ for Fe_3O_4@Cit and Fe_3O_4@PEI NPs, respectively.

Nano-sized metallic particles generally possess a high-surface energy and hence are more susceptible to the formation of aggregates in order to minimize their free energy. Though the passivated oxide layer provides a barrier to further oxidation, significant oxidation can still occur under prolonged exposure to air or aqueous media [31]. Therefore, in order to protect the particles from rapid oxidation and functionalize their surfaces with amino groups, the Al NPs are stabilized with APTES through a silanization reaction under reflux at 90 °C (Fig. 2(a)). Al NPs dispersed in a neutral-aqueous solution exhibit a thin Al_2O_3 shell (as seen in Fig. 1(a) inset) at which bare atoms of Al and O on the particle surface adsorb OH^- and H^+, respectively, to produce OH-rich surface. The –OH on the surface can react with APTES via the formation of silicon–oxygen–heteroatomic (Si–O–Al) bonds [32]. Zeta-potential measurement clearly shows that Al@APTES NPs are positively charged with a surface potential of +36.7 mV due to an abundance of amino groups anchored on the NP surface (Fig. 1(f)). The amine/carboxylic exchange was successively performed using GA, which resulted in functionalizing the particle surface with carboxylic groups (Fig. 2(a)). A negative-surface potential of −27 mV indicates the presence of carboxylic groups on the NP surface (Fig. 1(f)). Via TGA measurements in air, the contents of active aluminum in pristine Al, Al@APTES, and Al@APTES@GA samples were estimated to be 41.3%, 42.76%, and 39.7%, respectively, indicating that the stabilizing process has minimal impact on the oxidation state of NPs (Fig. S1). The dispersity of the functionalized Al NPs was investigated by dynamic-light scattering using zetasizer measurements (Fig. S2). The hydrodynamic size of Al@APTES NPs mostly ranges from 100 to 300 nm with a peak at ca. 164 nm, indicating that the NPs form nanoaggregates of 2–3 NPs. In the case of Al@APTES@GA NPs, the hydrodynamic size ranges from 59 to 200 nm, with a peak at ca. 91 nm, which indicates that most of the NPs are isolated. The higher dispersity and uniformity of Al@APTES@GA NPs (lower standard deviation and polydispersity indexes) compared to those of Al@APTES NPs is shown in the table in Fig. S2(c).

Analysis of FT-IR spectra confirms different surface stabilization of the NPs. Figure 2(b) shows the FT-IR spectra of the Al@APTES and Al@APTES@GA NPs. APTES is absorbed on the Al NPs surfaces by Al–O–Si bonds whose presence is proven by the stretching vibration at 1052 cm^{-1} [33]. The strong band at 1100 cm^{-1} is characteristic of Si–O–Si vibrations. Bands at 882 cm^{-1} and 1329 cm^{-1} are ascribed to the bending vibration of the $-NH_2$ group and stretching vibration of the C–N bond. The alkyl chain present in APTES molecules results in the appearance of typical bands at 2856, 2925, and 2970 cm^{-1}, attributed to CH stretching and a band at 1450 cm^{-1} due to CH_2–CH_2 stretching. After amine/carboxylic exchange with GA, the FTIR spectrum shows a characteristic carbonyl stretching vibration at 1745 cm^{-1}, indicating the presence of a carboxyl group on the surface. The band at 1611 cm^{-1} is characteristic of amide peaks and confirms that the exchange process

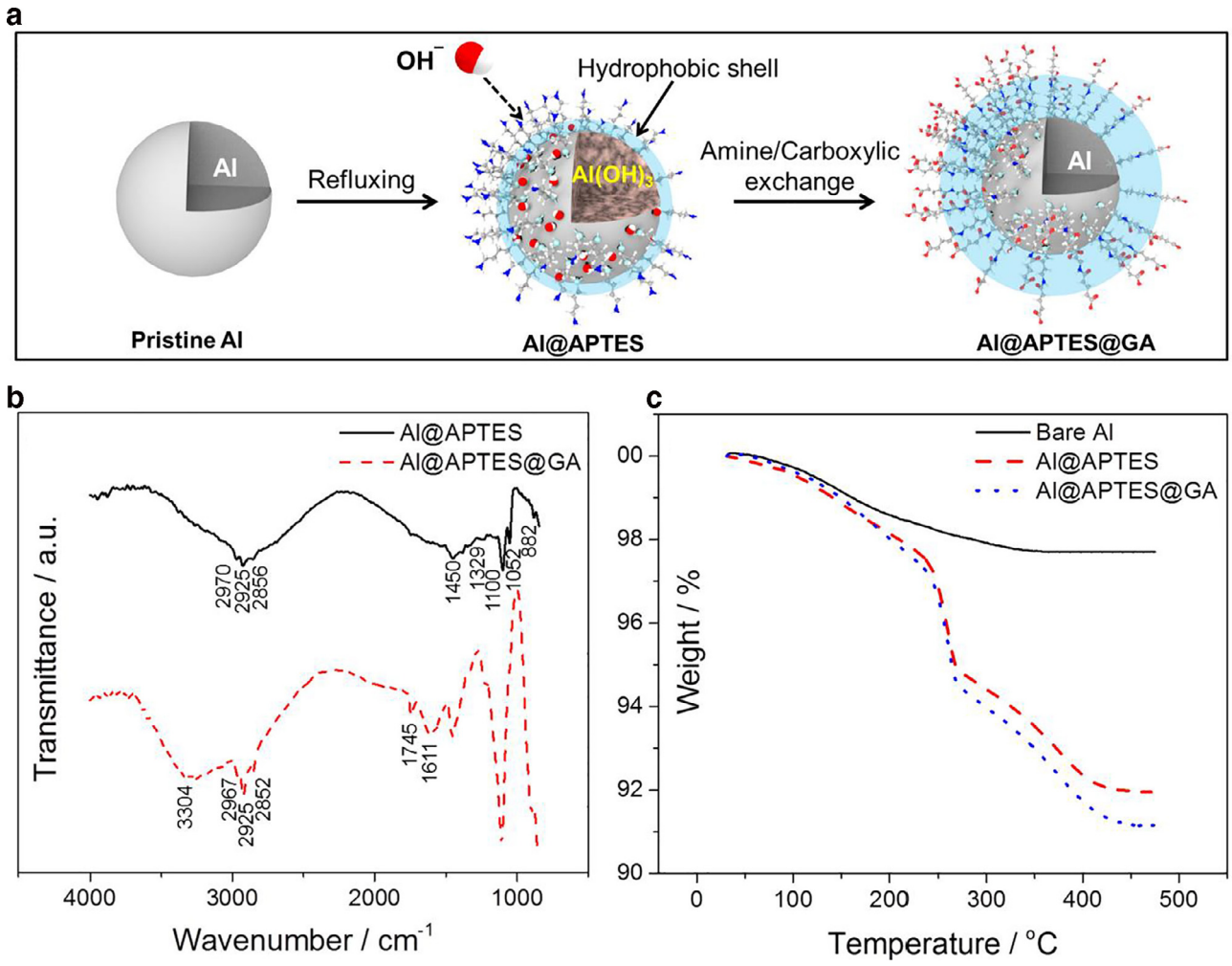

Fig. 2. Schematic illustration of stabilization of bare Al with APTES and GA (a). FTIR spectra (b) and TGA curves (c) of functionalized Al NPs.

was successful. The broad-absorption band at 3304 cm^{-1} can be attributed to O–H stretching modes. The presence of surfactants at the surfaces of the Al NPs was also revealed by thermogravimetric analysis (TGA), which was performed in nitrogen to prevent oxidation of aluminum. As shown in Fig. 2(c), bare Al NPs exhibit a small-weight loss of 2.3% probably related to removal of adsorbed water. The thermal profile of the Al@APTES sample shows three distinctive weight loss regions, the first in the 30–230 °C range due to the removal of adsorbed water, the second from 230 to 272 °C and the third from 272 to 433 °C, ascribed to the first and second steps of APTES decomposition [34]. The total weight loss of ca. 8% from the Al@APTES sample indicates that the mass ratio of APTES anchored on the Al surface is ca. 5.7%. On the other hand, there are four weight loss regions observed in the thermal profile of the Al@APTES@GA sample. The new weight loss region from 160 to 230 °C is attributed to the decomposition of GA, which triggers rapid weight loss around its boiling point (150 °C) [35]. The other weight loss regions are exactly the same as those in the profile of the Al@APTES sample. Greater weight loss of this sample (8.9%) also confirms the success of amine/carboxylic exchange process.

3.2. Stability of functionalized Al NPs

To evaluate the effect of coating layers on stability in aqueous media, suspensions of Al@APTES and Al@APTES@GA NPs were prepared in DI water. The size distributions of the colloids were measured using the zeta-sizer after storing the NPs at 25°C for 0, 6 and 12 h. As described above, the average sizes of the positively and negatively charged Al NPs right after dispersing by sonication (0 h) are 180 nm and 129 nm, respectively. The number of big aggregates (>500 nm) is insignificant in both cases. However, after 6 h of storage, though the color of the suspension has little change (Fig. S3(a)), the number of big aggregates (from 400 to 2300 nm) of Al@APTES increases remarkably. The peak in histogram exhibits a decrease in intensity and a shift in size from 164 nm to 220 nm. After 12 h of storage, a strong peak arises at 1281 nm, while the intensity of the smaller-size peak decreases and shifts to 295 nm (Fig. 3(a)). A transition in color from the original deep gray/black to white reveals a phase transformation (Fig. S3(a)). The color transition was accompanied with the occurrence of bubbles in the solvent, presumably from the evolution of hydrogen gas, indicating an oxidation process via electron donation from Al metal to H^+ [36]. In contrast, the suspension of Al@APTES@GA NPs shows almost no change in its size distribution curves and in the color of the suspension after 6 h or 12 h (Figs. 3(b) and S3(b)). An extensive study of the long-term stability of different functionalized Al NPs was performed in an aqueous solution at different storage temperatures. The zeta size and zeta potential of aqueous Al@APTES and Al@APTES@GA colloids stored at 40 and 60 °C are shown in Fig. 3(c) and (f). At 60 °C, the absolute-zeta potential of Al@APTES colloids rapidly decreases from 42 to 11 mV within 40 min, while their hydrodynamic size increases from 150 to 837 nm, accompanied with a color transition of the suspension. This indicates a fast-oxidation process (Fig. 2(e)). Though the colloids remain

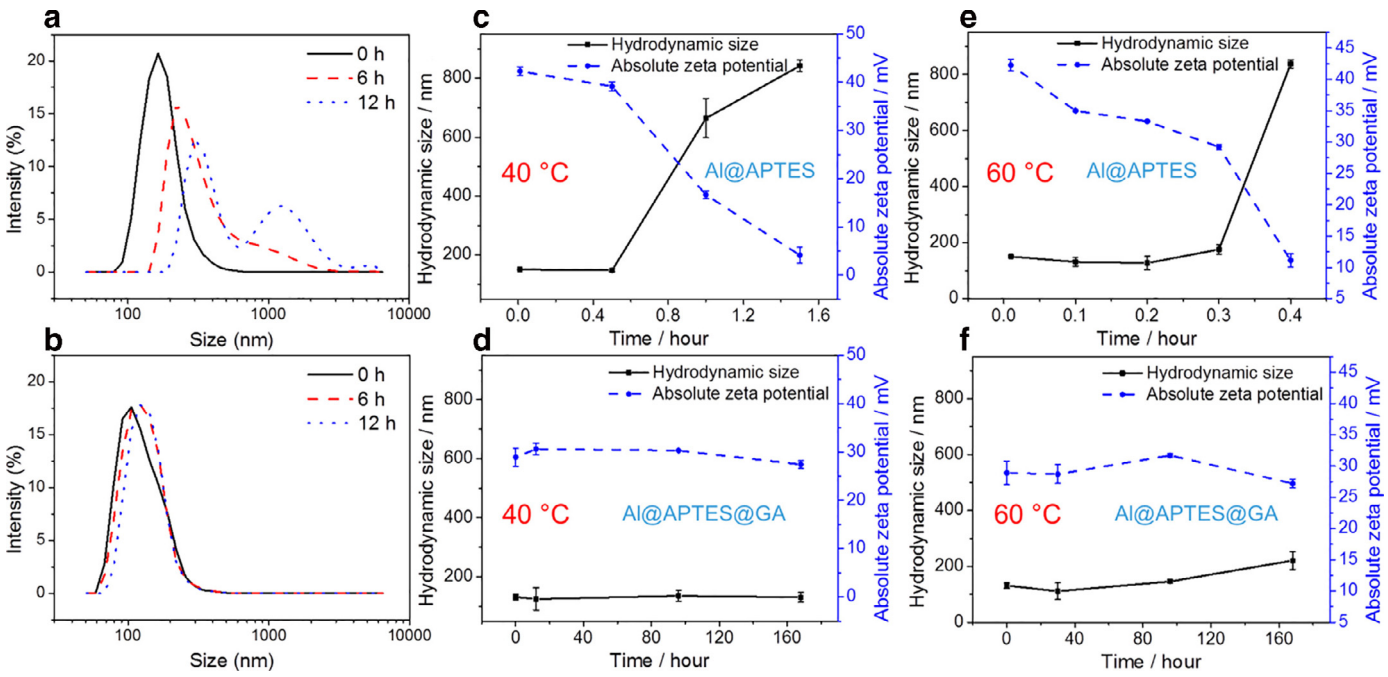

Fig. 3. Size distribution of Al@APTES (a) and Al@APTES@GA (b) NPs after 0, 6, and 12 h of storage in water at 25 °C. Zeta size (solid line) and absolute zeta potential (dotted line) of functionalized Al NPs in aqueous solution at 40 °C (c, d) and 60 °C (e, f).

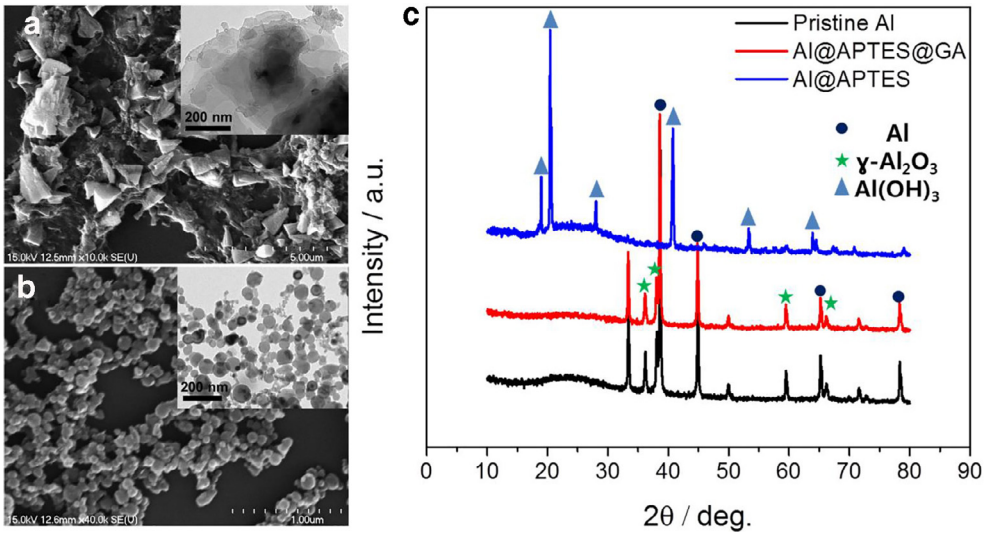

Fig. 4. SEM and TEM (inset) images of Al@APTES (a) and Al@APTES@GA (b) NPs after 12 h of storage at 25 °C. XRD patterns of as-received Al and Al@APTES and Al@APTES@GA NPs after 12 h of storage at 25 °C (c).

stable after storage at 40 °C for 40 min, sudden changes in the absolute-zeta potential and hydrodynamic size to 4 mV and 842 nm, respectively, accompanied by a color transition were observed after 90 min (Fig. 2(c)). Meanwhile, the absolute-zeta potential and hydrodynamic size of the Al@APTES@GA sample are nearly unchanged after storage for 7 days at 40 °C (Fig. 2(d)). After 7 days of storage at 60 °C, small decreases and increases of the absolute zeta potential (from 29 to 27.2 mV) and hydrodynamic size (from 131.5 to 221 nm), respectively (Fig. 2(f)), also indicate far better stability of Al@APTES@GA sample.

The morphologies of Al@APTES and Al@APTES@GA NPs after 12 h of storage at 25 °C in DI water are shown in Fig. 4(a) and (b). Al@APTES@GA NPs maintain the same morphology as pristine Al, while Al@APTES NPs appear completely different. There are no spherical particles remaining after complete oxidization (Fig. 4(a)). Instead, many micro-sized aggregates of various sizes and shapes are observed. XRD was used to investigate the compositions of the samples, which can reveal chemical processes taking place in the aqueous solution of Al@APTES NPs. XRD plots of as-received Al (pristine), Al@APTES and Al@APTES@GA NPs after 12 h of storage at 25 °C are shown in Fig. 4(c). Both the as-received and Al@APTES@GA samples present similar XRD patterns that indicate the existence of pure Al and γ-Al_2O_3 phases. This is consistent with the TEM image, where a thin layer of oxide was observed covering an Al core. However, the XRD pattern of the Al@APTES NPs shows that there no Al or Al_2O_3 phases remaining in the sample after 12 h of storage. Instead, all peaks correspond to bayerite ($Al(OH)_3$). The transformation of Al NPs to $Al(OH)_3$ in DI water is attributed to hydration reactions. Some simple potential aluminum hydration reactions in water are as follows [36,37]:

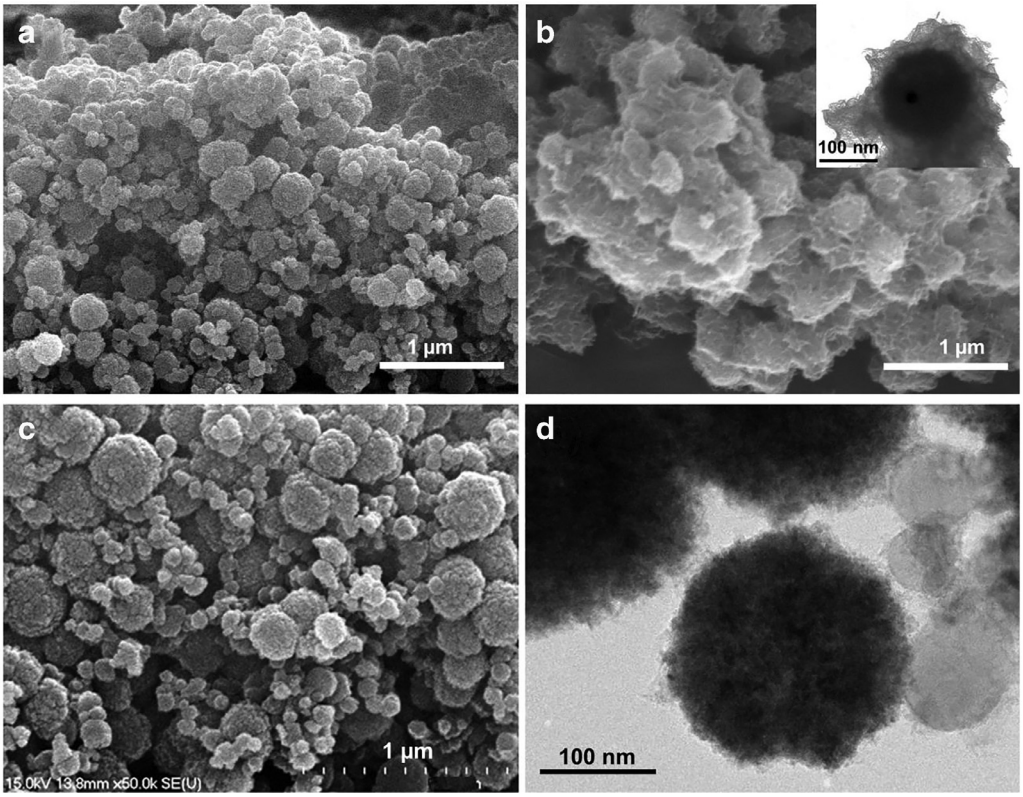

Fig. 5. Typical SEM and TEM ((b) inset and (d)) images of Magnerg composites composed of Al@APTES: 2 h- (a), 8 h- (b) assembly time and Al@APTES@GA: 8 h-assembly (c, d).

$$\gamma\text{-}Al_2O_3+3H_2O \rightarrow 2\beta\text{-}Al(OH)_3$$
$$Al + 3H_2O \rightarrow \beta - Al(OH)_3+3/2H_2$$

The superior stability of Al@APTES@GA NPs compared to Al@APTES in water is believed to be due to their bi-layer structure of stabilizer that effectively prevents diffusion of ions from water to the Al surface. It was reported that alkanesilane films can act as a water barrier [38]. The molecular structure of silane, processing protocol and the nature of the metal substrate all can affect the water-barrier performance, which critically governs the stability of Al NPs. Ng et al. and Grassi et al. have investigated the effects of the chain length and terminal functional groups of SAMs on their stability and protective properties [9,38]. They found that amino-terminated SAMs are very unstable if the alkyl chain is short (three carbon atoms long) but stable if the alkyl chain is long (eleven carbon atoms long). Hydrogen bonding between the hydrolyzed APTES molecules and aluminum oxide and among the hydrolyzed APTES molecules is believed to contribute to the instability of SAMs with short alkyl chains ($(CH_2)_3$) [9]. On the other hand, alkyl-terminated SAMs are very stable regardless of their alkyl chain length. However, the water-barrier effect of these alkyl-terminated SAMs is significantly enhanced when the chain length increases [38]. Though hydrophobically terminated SAMs were proven to be more effective in enhancing hydrolytic stability than hydrophilically terminated ones [39,40], they are inapplicable in aqueous media and do not facilitate the assembly process. If the alkyl chains of hydrophilically terminated SAMs are long (e.g., C18), they can add a strong hydrophobic layer to the NPs, which prevents proton diffusion to the particle surface, resulting in a reduction in surface potential [41]. In short, choosing a proper, moderate-length (C8 or more) surfactant for stabilization of Al NPs could both protect particles from hydrolysis and maintain a reasonably high surface potential. This could enhance dispersity and offer a great opportunity for applications in aqueous media.

3.3. Fabrication and performance of Magnerg composites

In order to assess the effect of functionalization on the reactivity of nanoenergetic materials, the Magnerg composites are fabricated through electrostatic interactions of oppositely charged particles, i.e., the negatively charged Fe_3O_4@Cit with the positively charged Al@APTES, or the positively charged Fe_3O_4@PEI with the negatively charged Al@APTES@GA. The morphologies of the Magnerg composites composed of Fe_3O_4@PEI and Al@APTES@GA after 2 h and 8 h assembly at 25 °C are shown in Fig. 5(a) and (b). In 2h-assembled sample, Fe_3O_4 and Al are quite frequently in close contact with each other due to strong electrostatic interaction. However, a completely different morphology is observed in 8 h-assembled sample. There is a layer that fully covers each particle, which has been confirmed to be $Al(OH)_3$ (Fig. 5(b)). On the other hand, the 8h-assembled sample composed of Al@APTES@GA exhibits identical morphology with the 2h-assembled sample of Al@APTES (Fig. 5(c)). TEM image in Fig. 5(d) clearly shows that high-interfacial contacts between the Fe_3O_4 and Al NPs have been achieved. This further indicates high stability of Al@APTES@GA NPs even in intimate contact with oxidizers.

A series of open burn tests were conducted to examine the explosive reactivity of the composites. Schematic illustration of combustion test setup is shown in Fig. 6(a). The ignition and explosion of the composites were monitored using a high-speed camera. Snapshots of the progress of ignition and explosion of three different Magnerg composites are shown in Fig. 6(b). The burn rates of the composites were calculated based on these snapshots. Here, the burn rates of samples were determined by taking the ratio of total propagation distance of the flame front

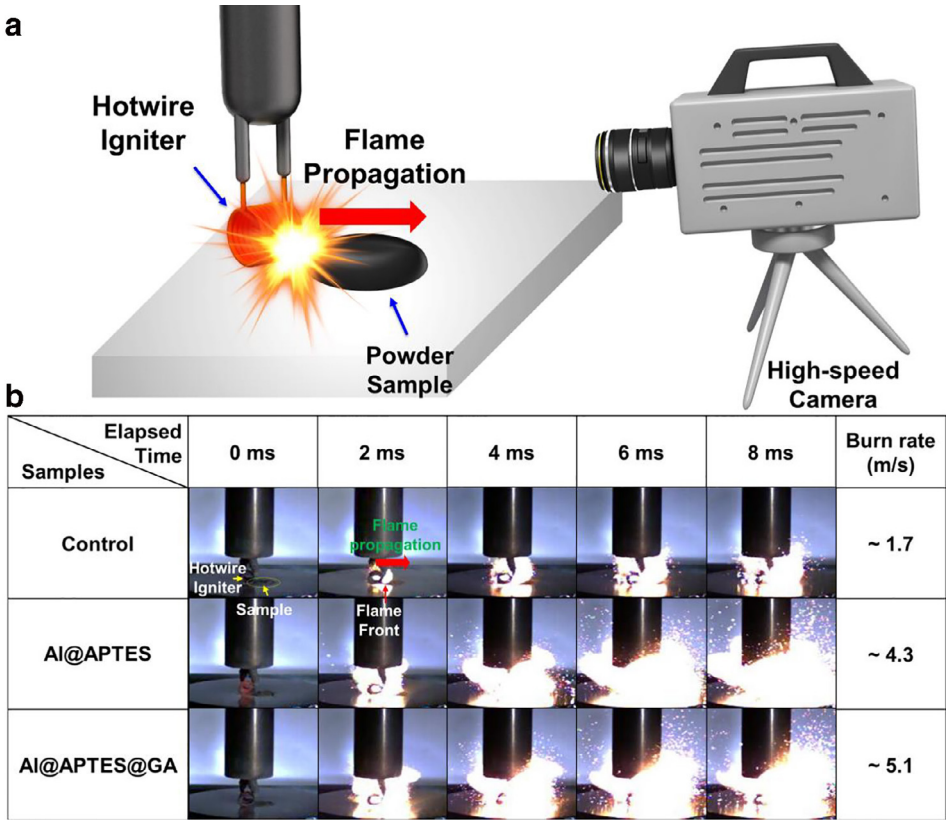

Fig. 6. Schematic illustration of combustion test setup (a) and high-speed camera snapshots for the control sample and two different Magnerg composites after 2 h assembly at 25 °C (b).

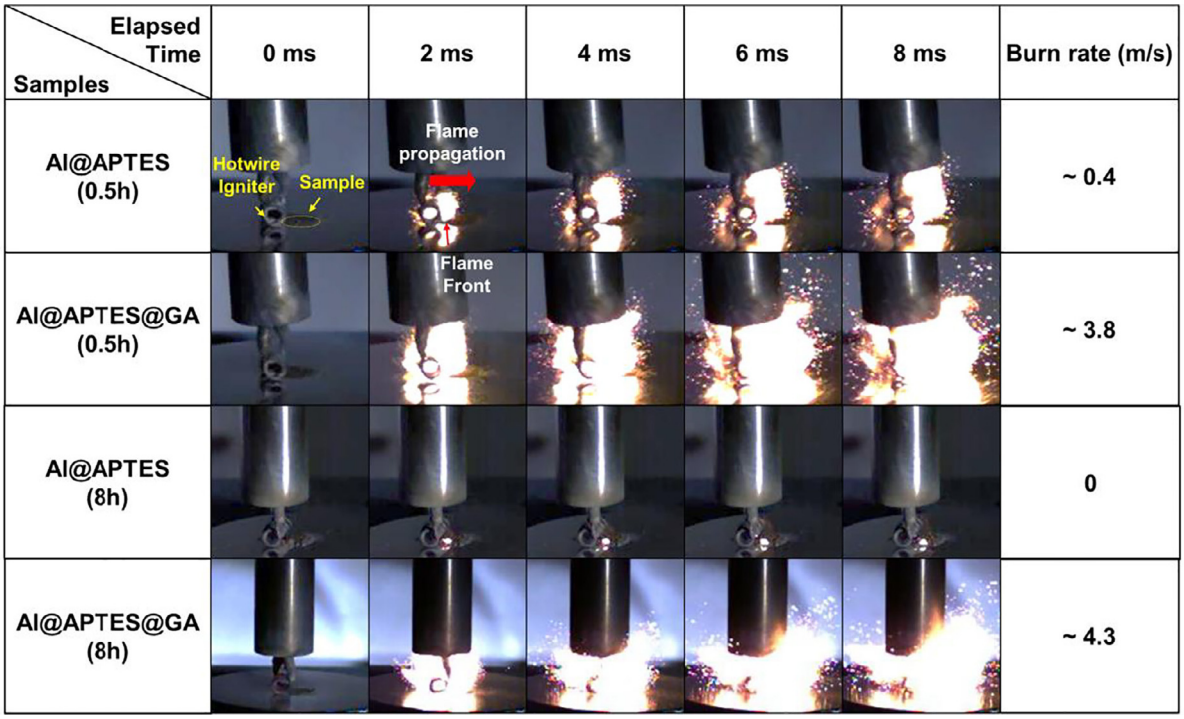

Fig. 7. High-speed camera snapshots of ignition and explosion progress of Magnerg composite composed of Fe_3O_4@Cit with Al@APTES and Fe_3O_4@PEI with Al@APTES@GA: assembly time 30 min and 8 h.

moving on the sample surface along the axis of sample length direction (i.e., total length of aligned powder) to the total time of flame propagation. A control sample composed of bare Al NPs was prepared by mixing two alcoholic suspensions to minimize electrostatic interaction. The burn rates of electrostatically assembled composites are remarkably higher than that of the control sample (~2.5 times for Al@APTES and ~3 times for Al@APTES@GA). This can be attributed to the well-arranged structure of Al–Fe_3O_4 composites prepared via the electrostatically induced assembly process. The self-propagating reaction of a mixed magnetite and aluminum powder produces iron and alumina, which is described by the reaction:

$$8Al + 3Fe_3O_4 \rightarrow 9Fe + 4Al_2O_3$$

It was reported that the reaction takes place immediately upon the melting of the Al core and involving the diffusion of aluminum ions onto the surface of the Al particle to come in contact with the surrounding oxidizers [42]. Therefore, the strong binding forces between Fe_3O_4 NPs and Al NPs resulted in shorter distances between Al NPs and Fe_3O_4 NPs and enhanced mass diffusion between Fe_3O_4 NPs and Al NPs so that the energetic reaction of the composites was more active. The lowest burn rate of the control sample compared to that of other samples can be attributed to poor dispersion of Al and Fe_3O_4 NPs. Also, the Al@APTES@GA sample exhibited a higher burn rate than Al@APTES sample. The higher stability of the suspension of Al@APTES@GA when compared to Al@APTES in DI water results in a better dispersion of Al and Fe_3O_4 NPs. The higher burn rate can also be attributed to the stabilizing layer of Al@APTES@GA preventing oxidation of Al particles during an assembly in an aqueous medium at 25 °C. The duration of the electrostatically induced assembly process was extended to 8 h in order to examine the effect of hydration of Al NPs on their explosive reactivity. In the case of the Al@APTES sample, because all Al have transformed to $Al(OH)_3$ phase, it is not surprising that the burn rate of the composite is zero. Meanwhile, there is a slight decrease in the burn rate (from 5.1 to 4.3 m/s) of the Al@APTES@GA sample assembled over 8 h (Fig. 7). Though assembly over a shorter period of time might diminish the oxidation effect, it results in an incomplete assembly process. Indeed, the burn rates of the Al@APTES and the Al@APTES@GA composites assembled over 30 min are 0.4 and 3.8 m/s, respectively, that are remarkably lower than those of composites assembled over 2 h (Fig. 7). Consequently, in addition to stability of Al NPs during assembly, relevant assembly duration is crucial to obtain optimal-energetic performance.

4. Conclusions

A simple and effective coating method was used to functionalize and protect the surfaces of Al NPs from oxidation and aggregation. It was found that APTES-functionalized Al NPs were unstable in an aqueous medium because of a hydration process, while GA-functionalized Al NPs exhibit long-term stability at elevated temperature. The superior stability of GA-functionalized Al NPs is ascribed to the bi-layer structure of their stabilizer. By increasing the intimacy between the fuel and oxidizer via electrostatic self-assembly, mass diffusion between the reactants and hence energetic reactivity was significantly enhanced. As a result of high stability and high dispersity of Al@APTES@GA NPs, their Magnerg composite exhibited highly energetic reactivity even after prolongated assembly process. Because of inherent magnetic property, the Magnerg composite and the direction of its explosion are expected to be manipulated by an external magnetic field, which could be promising for civil applications such as nanothermite cutters, building implosion or under-liquid explosions, as well as military applications. Further studies on combustion properties and magnetic field-directed explosion of the Magnerg composites are in progress and will be presented in a forthcoming paper.

Acknowledgments

This study was financially supported by the 2017 Post-Doc. Development Program of Pusan National University, The Civil & Military Technology Cooperation Program through the National Research Foundation of Korea (NRF) funded by the Ministry of Science, ICT & Future Planning (MSIP) (No. 2013M3C1A9055407) and the Commercializations Promotion Agency for R&D Outcomes (COMPA) funded by the MSIP (2016K000135).

Supplementary materials

Supplementary material associated with this article can be found, in the online version, at doi:10.1016/j.combustflame.2017.09.014.

References

[1] S. Borman, Advanced energetic materials emerge for military and space applications, Chem. Eng. News 72 (1994) 18–22.
[2] L. Meda, G. Marra, L. Galfetti, F. Severini, L. De Luca, Nano-aluminum as energetic material for rocket propellants, Mater. Sci. Eng. C 27 (2007) 1393–1396.
[3] K. Hara, T. Yoshida, T. Misawa, T. Maekawa, S. Yoshi, T. Yokoyama, T. Kazumi, M. Hayashi, Concept and performance of a non-Azide propellant for automotive airbag inflators, Propellants Explos. Pyrotech. 23 (1998) 28–33.
[4] R.J. Jouet, A.D. Warren, D.M. Rosenberg, V.J. Bellitto, K. Park, M.R. Zachariah, Surface passivation of bare aluminum nanoparticles using perfluoroalkyl carboxylic acids, Chem. Mater. 17 (2005) 2987–2996.
[5] H. Chen, J. Wang, Q. Huo, Self-assembled monolayer of 3-aminopropyltrimethoxysilane for improved adhesion between aluminum alloy substrate and polyurethane coating, Thin Solid Films 515 (2007) 7181–7189.
[6] M.L. Abel, J.F. Watts, R.P. Digby, The adsorption of alkoxysilanes on oxidised aluminium substrates, Int. J. Adhes. Adhes. 18 (1998) 179–192.
[7] Y.A. Atmane, L. Sicard, A. Lamouri, J. Pinson, M. Sicard, C. Masson, S. Nowak, P. Decorse, J.Y. Piquemal, A. Galtayries, Functionalization of aluminum nanoparticles using a combination of aryl diazonium salt chemistry and iniferter method, J. Phys. Chem. C 117 (2013) 26000–26006.
[8] C.A. Crouse, C.J. Pierce, J.E. Spowart, Influencing solvent miscibility and aqueous stability of aluminum nanoparticles through surface functionalization with acrylic monomers, ACS Appl. Mater. Interfaces 2 (2010) 2560–2569.
[9] A. Wang, H. Tang, T. Cao, S.O. Salley, K.S. Ng, In vitro stability study of organosilane self-assemble monolayers and multilayers, J. Colloid Interface Sci. 291 (2005) 438–447.
[10] G.M. Dutro, R.A. Yetter, G.A. Risha, S.F. Son, The effect of stoichiometry on the combustion behavior of a nanoscale Al/MoO_3 thermite, Proc. Combust. Inst. 32 (2009) 1921–1928.
[11] H. Wang, G. Jian, G.C. Egan, M.R. Zachariah, Assembly and reactive properties of Al/CuO based nanothermite microparticles, Combust. Flame 161 (2014) 2203–2208.
[12] W. Zhang, B. Yin, R. Shen, J. Ye, J.A. Thomas, Y. Chao, Significantly enhanced energy output from 3D ordered macroporous structured Fe_2O_3/Al nanothermite film, CS Appl. Mater. Interfaces 5 (2013) 239–242.
[13] D. Xu, Y. Yang, H. Cheng, Y.Y. Li, K. Zhang, Integration of nano-Al with Co_3O_4 nanorods to realize high-exothermic core–shell nanoenergetic materials on a silicon substrate, Combust. Flame 159 (2012) 2202–2209.
[14] M.L. Pantoya, J.J. Granier, Combustion behavior of highly energetic thermites: nano versus micron composites, Propellants Explos. Pyrotech. 30 (2005) 53–62.
[15] T.M. Tillotson, A.E. Gash, R.L. Simpson, L.W. Hrubesh, J.H. Satcher, J.F. Poco, Nanostructured energetic materials using sol–gel methodologies, J. NonCryst. Solids 285 (2001) 338–345.
[16] J.Y. Malchi, T.J. Foley, R.A. Yetter, Electrostatically self-assembled nanocomposite reactive microspheres, ACS Appl. Mater. Interfaces 1 (2009) 2420–2423.
[17] K.J. Blobaum, M.E. Reiss, J.M. Plitzko, T.P. Weihs, Deposition and characterization of a self-propagating CuO_x/Al thermite reaction in a multilayer foil geometry, J. Appl. Phys. 94 (2003) 2915–2922.
[18] S.H. Kim, M.R. Zachariah, Enhancing the rate of energy release from nanoenergetic materials by electrostatically enhanced assembly, Adv. Mater. 16 (2004) 1821–1825.
[19] R. Thiruvengadathan, S.W. Chung, S. Basuray, B. Balasubramanian, C.S. Staley, K. Gangopadhyay, S. Gangopadhyay, A versatile self-assembly approach toward high performance nanoenergetic composite using functionalized graphene, Langmuir 30 (2014) 6556–6564.
[20] J.Y. Ahn, J.H. Kim, J.M. Kim, D.W. Lee, J.K. Park, D. Lee, S.H. Kim, Combustion characteristics of high-energy Al/CuO composite powders: the role of oxidizer structure and pellet density, Powder Technol. 241 (2013) 67–73.
[21] J.M. Slocik, L.F. Drummy, M.B. Dickerson, C.A. Crouse, J.E. Spowart, R.R. Naik, Bioinspired high-performance energetic materials using heme-containing crystals, Small 11 (2015) 3539–3544.

[22] R. Shende, S. Subramanian, S. Hasan, S. Apperson, R. Thiruvengadathan, K. Gangopadhyay, S. Gangopadhyay, P. Redner, D. Kapoor, S. Nicolich, Nanoenergetic composites of CuO nanorods, nanowires, and Al-nanoparticles, Propellants, Explos., Pyrotech. 33 (2008) 122–130.
[23] F. Séverac, P. Alphonse, A. Estève, A. Bancaud, C. Rossi, High-energy Al/CuO nanocomposites obtained by DNA-directed assembly, Adv. Funct. Mater. 22 (2012) 323–329.
[24] nd P. Brito, L. Durães, J. Campos, A. Portugal, Simulation of Fe_2O_3/Al combustion: sensitivity analysis, Chem. Eng. Sci. 62 (2007) 5078–5083.
[25] P.M. Botta, P.G. Bercoff, E.F. Aglietti, H.R. Bertorello, J.P. López, Magnetic and structural study of mechanochemical reactions in the Al–Fe_3O_4 system, J. Mater. Sci. 37 (2002) 2563–2568.
[26] N.I. Wakayama, Effect of a gradient magnetic field on the combustion reaction of methane in air, Chem. Phys. Lett. 188 (1992) 279–281.
[27] N.I. Wakayama, Magnetic promotion of combustion in diffusion flames, Combust. Flame 93 (1993) 207–214.
[28] J. Baker, M.E. Calvert, A study of the characteristics of slotted laminar jet diffusion flames in the presence of non-uniform magnetic fields, Combust. Flame 133 (2003) 345–357.
[29] S. Swaminathan, Effects of magnetic field on micro flames Master Thesis, Louisiana State University, 2005.
[30] J. Mohler and T.W. Mohler, Thermite torch cutting nozzle, Google Patents US6805832 B2, (2004).
[31] A.A. Gromov, U. Föter-Barth, U. Teipel, Aluminum nanopowders produced by electrical explosion of wires and passivated by non-inert coatings: characterisation and reactivity with air and water, Powder Technol 164 (2006) 111–115.
[32] L.A. Prado, M. Sriyai, M. Ghislandi, A. Barros-Timmons, K. Schulte, Surface modification of alumina nanoparticles with silane coupling agents, Braz, Chem. Soc. 21 (2010) 2238–2245.
[33] S.D. Ross, Inorganic infrared and Raman spectra, McGraw-Hill, London, 1972.
[34] L. Etgar, G. Schuchardt, D. Costenaro, F. Carniato, C. Bisio, S.M. Zakeeruddin, M.K. Nazeeruddin, L. Marchese, M. Graetzel, Enhancing the open circuit voltage of dye sensitized solar cells by surface engineering of silica particles in a gel electrolyte, J. Mater. Chem. A 1 (2013) 10142–10147.
[35] D.V. Leff, L. Brandt, J.R. Heath, Synthesis and characterization of hydrophobic, organically soluble gold nanocrystals functionalized with primary amines, Langmuir 12 (1996) 4723–4730.
[36] S. Kanehira, S. Kanamori, K. Nagashima, T. Saeki, H. Visbal, T. Fukui, K. Hirao, Controllable hydrogen release via aluminum powder corrosion in calcium hydroxide solutions, J. Asian Cer. Soc. 1 (2013) 296–303.
[37] G. Lefevre, M. Duc, P. Lepeut, R. Caplain, M. Fédoroff,, Hydration of g-alumina in water and its effects on surface reactivity, Langmuir 18 (2002) 7530–7537.
[38] A. Frignani, F. Zucchi, G. Trabanelli, V. Grassi, Protective action towards aluminium corrosion by silanes with a long aliphatic chain, Corros. Sci. 48 (2006) 2258–2273.
[39] J. Genzer, K. Efimenko, Creating long-lived superhydrophobic polymer surfaces through mechanically assembled monolayers, Science 290 (2000) 2130–2133.
[40] T. Nihei, S. Kurata, Y. Kondo, K. Umemoto, N. Yoshino, T. Teranaka, Enhanced hydrolytic stability of dental composites by use of fluoroalkyltrimethoxysilanes, J. Dent. Res. 81 (2002) 482–486.
[41] J. Wang, G. Meng, K. Tao, M. Feng, X. Zhao, Z. Li, H. Xu, D. Xia, J.R. Lu, Immobilization of lipases on alkyl silane modified magnetic nanoparticles: effect of alkyl chain length on enzyme activity, PloS One 7 (2012) e4347.
[42] S. Chowdhury, K. Sullivan, N. Piekiel, L. Zhou, M.R. Zachariah, Diffusive vs explosive reaction at the nanoscale, J. Phys. Chem. C 114 (2010) 9191–9195.